Metal-silicate partitioning of Re, Ru, Pt, Os, Ti, Nb, and Ta in reduced differentiated planetary bodies. K. Righter[1], S. Yang [2], M. Humayun[2], A. Boujibar[3], R. Rowland II [4,5]and K. Pando[4]; [1] NASA JSC, Mailcode XI2, 2101 NASA Pkwy, Houston, TX 77058; kevin.righter-1@nasa.gov; [2] National High Magnetic Field Laboratory, Florida State Univ., Tallahassee, FL 32310; [3] Earth and Planets Laboratory, Carnegie Institution for Science, 5251 Broad Branch Road NW, Washington DC 20015-1305; [4] Jacobs JETS Contract, NASA JSC, Houston, TX 77058; [5] Los Alamos National Laboratory, Mail Stop P952, Los Alamos, NM 87545, USA.

Introduction: Siderophile (iron-loving) elements are strongly fractionated during differentiation of planetary bodies into core and mantle [1]. Because the fractionation is controlled by pressure, temperature, redox conditions, and composition, this group of elements can provide important constraints on the conditions of accretion and core formation in early solar system bodies (planetesimals) and planets (Earth, Mercury, Venus)[2]. At the reducing conditions thought to prevail in the early solar system, Si is known to alloy with FeNi metallic liquids (e.g., [3]) affecting the activity coefficients of siderophile elements in FeNi liquids and thus ultimately their partitioning behavior between metal and silicate melts. The effect of Si on some siderophile elements can be significant (e.g., [4]: Ni, Co; [5,6]: Ge, As, Sb, Pd, Pt, Au). The effect of Si has not yet been determined for several key siderophile elements including the highly siderophile Re, Ru and Os, and the weakly siderophile Ta, Nb, and Ti. Here, we report new experiments designed to quantify the effect of Si on the partitioning of Re, Pt, Os, Ru, Ti, Ta and Nb between metal and silicate melts. The results will be used to evaluate metal/silicate equilibrium for Nb, Ta, Ti and Nb/Ta ratios in planetary mantles, mantle concentrations of Ru, Re, Pt, and Os during accretion, the evolution of Re/Os, Pt/Os ratios in magma oceans, and the role of a late veneer in establishing Re and Ru abundances in the terrestrial mantle.

Experimental approach: Experiments were carried out in a non-end-loaded piston cylinder apparatus under run conditions of 1 GPa and 1600 ºC. Samples were heated with a graphite furnace, and pressure imposed on the samples using a $BaCO_3$ pressure transmitting medium using approaches and calibrations described previously [6]. Starting materials comprised of basaltic silicate (70% by mass; Knippa basalt; [7]) mixed with metal of three different compositions (and hence three different series): metallic Fe + 5% Re, metallic Fe + 5% Ru, and metallic Fe + 5% each of Re, Pt, and Os. Silicon metal was also added to the metallic mixture at 2, 4, 6, 8, and 10 %, to create variable amounts of Si alloyed with Fe in each series. The metal mixtures were added so that the total metallic fraction was 30% by mass. These metal-silicate mixtures were then placed in sintered MgO capsules. At run conditions, the MgO capsule reacts with the silicate melt to form more MgO-rich liquids that have 22-26 wt% MgO. Samples were held at run conditions for 90 minutes at 1600 °C to ensure approach to equilibrium, with the duration determined by a previously completed series of experiments on siderophile elements [5].

Analytical approach: Experimental metals and silicates were analyzed using a combination of electron microprobe analysis (EMPA) at NASA-JSC, and laser ablation ICP-MS at Florida State University. EMPA analysis (using both Cameca SX100 and JEOL 8530 FEG microprobes) was used for major and minor elements (Fe, Si, P, Re, Ru, and S) and utilized a variety of mineral and glass standards with 15 kV and 20 nA conditions. Trace elements Re, Pt, Os, Ru, Ta, Ti, Nb (typically < 100 ppm) were measured with LA-ICP-MS using glass and metal standards and either spot or line analyses depending on the size of the metal or silicate regions of interest. Each sample was analyzed by an ElectroScientific Instruments (ESI) New Wave™ UP193FX excimer (193 nm) laser ablation system coupled to a Thermo Element XR™ Inductively Coupled Plasma Mass Spectrometer (ICP-MS) at the Plasma Analytical Facility of the National High Magnetic Field Laboratory, Florida State University. Peaks analyzed were: ^{29}Si, ^{31}P, ^{47}Ti, ^{51}V, ^{53}Cr, ^{55}Mn, ^{57}Fe, ^{59}Co, ^{60}Ni, ^{63}Cu, ^{66}Zn, ^{71}Ga, ^{93}Nb, ^{102}Ru, ^{103}Rh, $^{105+106}$Pd, ^{181}Ta, ^{182}W, ^{185}Re, ^{190}Os, ^{193}Ir, ^{195}Pt, ^{197}Au, ^{208}Pb, and other elements as described by [8]. Laser fluence was 2 GW/cm^2, and internal standards were ^{29}Si for silicates and ^{57}Fe for metal+sulfide. Relevant isobaric interferences were addressed according to [8] and relative sensitivity factors were obtained using NIST SRM 610 glass, USGS Basaltic Glasses BHVO-2G, BIR-1G, and BCR-2G for lithophile elements [9], and Hoba IVB [10] and Filomena IIA [11] for siderophile elements [12-14]. Laser modes of 75 μm lines on metals and 50 μm spots or 75 μm lines on silicates, allowed good precision while silicate analyses could also could be screened for HSE spikes associated with entrained metal particles or nuggets. The relative standard deviation (RSD) of HSE abundances in metal from each of the runs was ~ 2 %, and RSD of HSE in the silicate portions averaged ~ 20 %.

Results: Metallic liquid and silicate melt were equilibrated in each experiment. Because Si metal was added to the metal phase, and Si content will cause lower fO_2, oxygen fugacities ranged from IW-1.8 for Si-free runs compared to as low as IW-7.8 for Si-bearing runs (where oxygen fugacity was calculated relative to the

iron-wüstite (IW) oxygen buffer using the expression $\Delta IW = -2\log [X_{Fe}/X_{FeO}]$. Measured P, Ru, Re, Pt, Os, Ti, Nb, and Ta concentrations in metal and silicate were used to calculate the metal (met) - silicate (sil) exchange coefficient K_d according to this equation:

$$MOn/2_{sil} + (n/2)Fe_{met} = M_{met} + (n/2)FeO_{sil} \quad (1)$$

From these equilibria the interaction parameter ε_M^{Si} [15] can be calculated and used to isolate the effect of a solute (such as Si) in Fe metallic liquid on the activity of a trace element (e.g., [5,6]). Positive values of ε_M^{Si} will cause an increase in activity coefficient and thus a decrease in D(metal/silicate), while a negative ε_M^{Si} will cause a decrease in activity coefficient and thus an increase in D(metal/silicate). Determination of ε_M^{Si} is thus very useful in constraining the effect of alloyed Si in the core on the metal-silicate behavior of siderophile elements. Using this approach, we have determined ε_M^{Si} for Re (45±7 and 50±17 in two different series), Ru (44±8), Pt (29±8), Os (43±16), P (70±15), Ti (10±3), Nb (45±8), and Ta (45±7). All elements have positive epsilon parameters, indicating that dissolved Si causes a decrease in their metal-silicate partition coefficients (Fig. 1). These new values for Re, Ru, Pt, Os, P, Ti, Nb, and Ta demonstrate that D(metal/silicate) will be reduced for all elements with the addition of Si to the metallic liquid. Furthermore, the effect of Si is much stronger than the effect of S for Re and Ru, commonly thought to exhibit chalcophile behavior. Silicon in the metal causes a decrease in D(metal/silicate) whereas S in the metal causes an increase (i.e., these are truly chalcophile elements; Fig. 1).

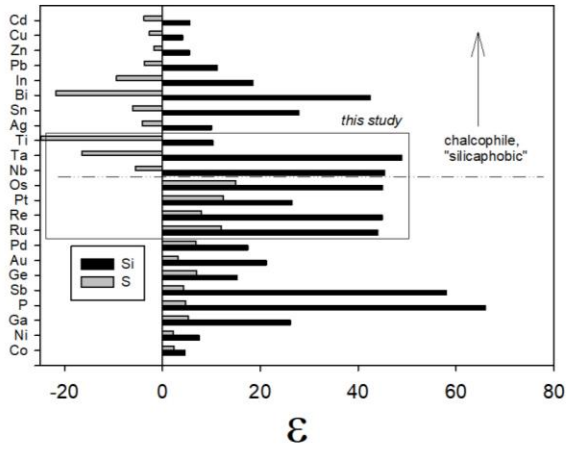

Figure 1: Summary of epsilon interaction parameter values for elements in this study and compared to previously determined values [4,5,6,16,17].

Implications: Using previous accretion and core-mantle equilibrium modelling approaches [6], the mantle abundances of these elements resulting from metal-silicate equilibrium can be calculated in several scenarios for a deep molten early Earth. Concentrations of Pt and Os in the mantle become too high at the conditions of a deep magma ocean, and require a removal mechanism such as reduction involving segregation of metal to the base of the magma ocean (by accretion of reduced material, or an internal reduction process), or segregation of a late sulfide matte. A late reduction event can effectively remove Pt and Os to levels close to those in the BSE, but would require that such a small fraction of metal can efficiently segregate through the mantle. Separation of a sulfide matte at the base of a deep magma ocean is possible as long as the magma ocean crystallizes to at least 50% and the extent of sulfide segregation is ~ 0.2 to 1.5 %. Any sulfide matte model must also be consistent with the chalcophile elements Ni, Cu, and Bi, whose concentrations will also decrease with the segregation of such a matte. On the other hand, Re and Ru have concentrations far below the BSE levels, and would become even lower with sulfide matte or metal segregation. Sulfide segregation would also leave the mantle with low abundances, and non-chondritic ratios, of Au, Pd, and Pt [6].

An explanation for the near chondritic relative ratios of the HSE could be provided by a combination of sulfide matte plus late veneer, or metal segregation plus late veneer. Either scenario ultimately involves a three stage process for explaining HSEs in the BSE – (a) accretion and metal-silicate equilibrium, (b) removal by metal or sulfide, and (c) addition by a late veneer. The results for Ru will be considered with respect to Mo and Ru isotopic constraints on accretion stages [18,19].

References: [1] Walker, R.J. (2009) Geochem. 69, 101-125; [2] Righter, K. (2016) Deep Earth: Physics and Chemistry of the Lower Mantle and Core, AGU Monogr. 217, 161-178; [3] Hirose, K. (2013) AREPS 41, 657-691; [4] Tuff, J. et al. (2011) GCA 75, 673-690; [5] Righter, K. et al. (2017) EPSL 198, 1-16; [6] Righter, K. et al. (2018) GCA 232, 101-123; [7] Lewis, R.D. et al. (1993) Met. 28, 622-628; [8] Yang, S. et al. (2015) MaPS 50, 691-714; [9] Jochum, K.-P. et al. (2011) Geost. Geoanal. Res. 35, 397-429; [10] Walker, R.J. et al. (2008) GCA 72, 2198-2216; [11] Wasson, J.T. et al. (1989) GCA 53, 735-744; [12] Humayun, M. et al. (2007) GCA 71, 4609-4627; [13] Gaboardi, M. and Humayun, M. (2009) J. Anal. Atom. Spectr. 24, 1188-1197; [14] Humayun, M. (2012) MaPS 47, 1191-1208; [15] Lupis, C.H.P. (1983) Chemical Thermodynamics of Materials. Elsevier, 581 pp; [16] Wood, B.J. et al. (2014) GCA 145, 248-267; [17] Righter, K. et al. (2019) MaPS 54, 1379-1394; [18] Budde, G. et al., (2019) Nat. Astro. 3, 736-741; [19] Hopp, T. et al. (2020) EPSL 534, p.116065.